Supplementary Information

Nonreciprocal quantum photon-pair source with chiral ferroelectric nematics

Jin-Tao Pan[1,6], Yun-Kun Wu[2,3,4,6], Ling-Ling Ma[1,6,*], Ning Wang[1], Xin-Yu Tao[1], Bo-Han Zhu[1], Shu Wang[2,3,4], Fang-Wen Sun[2,3,4], Guang-Can Guo[2], Hui Jing[5,*], Xi-Feng Ren[2,3,4,*] & Yan-Qing Lu[1,*]

[1]National Laboratory of Solid State Microstructures, Key Laboratory of Intelligent Optical Sensing and Manipulation, Collaborative Innovation Center of Advanced Microstructures, College of Engineering and Applied Sciences, Nanjing University, Nanjing, China.
[2]CAS Key Laboratory of Quantum Information, University of Science and Technology of China, Hefei, China.
[3]CAS Synergetic Innovation Center of Quantum Information and Quantum Physics, University of Science and Technology of China, Hefei, China.
[4]Hefei National Laboratory, University of Science and Technology of China, Hefei, China.
[5]Key Laboratory of Low-Dimensional Quantum Structures and Quantum Control of Ministry of Education, Department of Physics and Synergetic Innovation Center for Quantum Effects and Applications, Hunan Normal University, Changsha, China.
[6]These authors contributed equally: Jin-Tao Pan, Yun-Kun Wu, Ling-Ling Ma.
*e-mail: malingling@nju.edu.cn; jinghui@hunnu.edu.cn; renxf@ustc.edu.cn; yqlu@nju.edu.cn.

Keywords: liquid crystal; quantum entanglement; photon-pair generation; phase matching; nonreciprocity

Section 1: Optical rotatory effect of the helical FNLC

We provide the theoretical framework for polarized light propagation in chiral ferroelectric nematic liquid crystal (FNLC). The theoretical model mainly includes the polarization rotation dynamics of the pump field (*p*), signal field (*s*) and idle field (*i*). We approximate the fields to be paraxially propagating along the longitudinal *z* axis.

The FNLC of length *L* and second-order nonlinear susceptibility $\chi^{(2)}$ is placed perpendicular to the *z* axis, and the FNLC input face is used to define $z = 0$. The electric fields are denoted by $\boldsymbol{E}_j(z)$, where $j = p$, i, and s, respectively. The electric field is defined as

$$\boldsymbol{E}_j(z) = \begin{pmatrix} A_{j,x}(z) \\ A_{j,y}(z) \end{pmatrix} e^{ik_j z}, \tag{1}$$

where $k_j = n_j \omega_j / c$ is the wavevector, c is the speed of light in vacuum, n_j is the refractive index, ω_j is the angular frequency. In the helical ferroelectric fluid, the polar vector undergoes a rotation that is linearly related to orientational angle $\theta(z)$, which is governed by the helical structure of the chiral FNLC structure:

$$\theta(z) = Gz + \theta_{\text{head}}, \tag{2}$$

where θ_{head} is the alignment angle of the head plane, G is the reciprocal vector provided by the continuous sinusoidal modulation, defined as $G = 2\pi / p$, where p is the helical pitch. The polar LC director field of the right-handed chiral FNLC are given by

$$\mathbf{n}(z) = \begin{pmatrix} \cos(Gz + \theta_{\text{head}}) \\ \sin(Gz + \theta_{\text{head}}) \end{pmatrix}. \tag{3}$$

In order to simplify the model, the alignment direction of the liquid crystal director at the head plane is along the *x*-axis. The helical anisotropic medium is divided into *N* layers under the assumption that each layer is a wave plate with a certain phase delay, own azimuthal angle and thickness d_i (i = 1, 2, …, N). The propagation of the polarized light is then considered in terms of the multiplication of Jones matrices, and assuming that the number of plates tends to infinity (correspondingly, the thickness d_i of each film tends to zero). The amplitude is given by the simplified equations[1]:

$$\begin{pmatrix} A_{j,x}(z) \\ A_{j,y}(z) \end{pmatrix} = e^{-ik_j z} \boldsymbol{R}(z) \boldsymbol{M}_j(z) \begin{pmatrix} A_{j,x}(0) \\ A_{j,y}(0) \end{pmatrix}, \tag{4}$$

where $\boldsymbol{R}(z)$ is the rotation matrix:

$$\boldsymbol{R}(z) = \begin{pmatrix} \cos\Phi(z) & -\sin\Phi(z) \\ \sin\Phi(z) & \cos\Phi(z) \end{pmatrix}; \tag{5}$$

$\Phi(z) = \theta(z) - \theta_{\text{head}} = Gz$ is the relative rotation angle. And

$$\boldsymbol{M}_j(z) = \cos\Theta(z) \cdot \boldsymbol{I} + \operatorname{sinc}\Theta(z) \begin{pmatrix} -i\Gamma_j(z)/2 & \Phi(z) \\ -\Phi(z) & i\Gamma_j(z)/2 \end{pmatrix} \tag{6}$$

is the matrix of polarized light propagation through the helical anisotropic medium, $\boldsymbol{I}$ is the identity matrix, $\operatorname{sinc}(\cdots) \equiv \frac{\sin(\cdots)}{\cdots}$ is the sinc function, $\Gamma_j(z) = 2\pi\Delta n_j z / \lambda_j$ is the phase retardation, λ is the wavelength of the light, $\Delta n_j = n_{j,\text{e}} - n_{j,\text{o}}$ is the birefringence, $n_{j,\text{e}}$ and $n_{j,\text{o}}$ are the extraordinary and ordinary refractive

indices, respectively, and $\Theta(z)=\sqrt{\Phi^2+[\Gamma_j(z)/2]^2}$. Substituting Eqs. (5) and (6) into (4), and assuming that $\Delta n_j p \gg \lambda_j$, we obtain

$$\begin{pmatrix} A_{j,x}(z) \\ A_{j,y}(z) \end{pmatrix} = e^{-ik_j z} \begin{pmatrix} \cos\Phi(z)e^{-i\Gamma_j(z)/2} & -\sin\Phi(z)e^{i\Gamma_j(z)/2} \\ \sin\Phi(z)e^{-i\Gamma_j(z)/2} & \cos\Phi(z)e^{i\Gamma_j(z)/2} \end{pmatrix} \begin{pmatrix} A_{j,x}(0) \\ A_{j,y}(0) \end{pmatrix}. \quad (7)$$

The polarization evolution during its propagation through the LC medium can be calculated by Eq. (7). As shown in **Fig. S1a**, we show the polarization evolution of vertical (V), horizontal (H), left-handed circular (L), and right-handed circular (R) polarized pumping light. If the wave that is incident on a medium with linear polarization, which is parallel to the polar direction of the head plane ($\left(A_{j,x}(0), A_{j,y}(0)\right)^T = (1,0)^T$), the polarization vector of the wave at the exit plane ($z = L$) is

$$\begin{pmatrix} A_{j,x}(L) \\ A_{j,y}(L) \end{pmatrix} = e^{-i\left[k_j L+\Gamma_j(L)/2\right]} \begin{pmatrix} \cos\Phi(L) \\ \sin\Phi(L) \end{pmatrix}. \quad (8)$$

This indicates that the polarization remains parallel to the director as the light propagates through the chiral LC medium. When the incident light $\left(A_{j,x}(0), A_{j,y}(0)\right)^T = (0,1)^T$ is linearly polarized perpendicular to the director at the entry plane, the polarization, $\left(A_{j,x}(L), A_{j,y}(L)\right)^T = e^{-i\left[k_j L-\Gamma_j(L)/2\right]}\left(-\sin\Phi(L), \cos\Phi(L)\right)^T$, remains perpendicular to the director as the light propagates through the LC. Interestingly, if the input wave is a circular polarization, it changes from circular, elliptical polarization, to linear, reverse-handed elliptical polarization and so on, as it propagates in the helical FNLC.

Note that this conclusion is obtained under the $\Delta n_j p \gg \lambda_j$ approximation. We calculated the polarization evolution using the experimental parameters, as shown in **Fig. S1b**. Although the V (H) linear polarization does not strictly maintain the linear polarization state, most of the polarization components are still parallel (perpendicular) to the local polar director, so the above conclusion is still understandable.

Section 2: SPDC in helical phase matched FNLC.

The quantum state of photon pairs generated at $z = z_0$ by SPDC could be represented as[2]

$$\left|\psi(z_0)\right\rangle = \sum_{lmn} \zeta_{lmn}(z_0)\hat{a}^{\dagger}_{i,m}\hat{a}^{\dagger}_{s,n}e^{i\Delta k z_0}\left|0\right\rangle, \tag{9}$$

where $l, m, n = \{x, y, z\}$ represent the global coordinate system; $\hat{a}^{\dagger}_{i,m}$ and $\hat{a}^{\dagger}_{s,n}$ are generation operators of signal and idle photons along n- and m-axes, respectively; $\zeta_{lmn}(z_0) \propto \chi^{(2)}_{lmn}(z_0)E_{p,l}(z_0)$ is the nonlinear conversion coefficient, $\chi^{(2)}_{lmn}(z_0)$ is the second-order nonlinear susceptibility, Δk represents the phase-mismatch. In the case of collinear helical quasi-phase-matching the mismatch is

$$\Delta k_{\mathrm{HPM}} = 2\pi\left(\frac{n_p}{\lambda_p} - \frac{n_s}{\lambda_s} - \frac{n_i}{\lambda_i} - \frac{2\pi}{p}\right). \tag{10}$$

FNLCs exhibit strong nonlinear optical responses with non-zero second-order nonlinear optical susceptibility $\chi^{(2)}_{\mathrm{aaa}} = 11.2\ \mathrm{pm{\cdot}V^{-1}}$ and $\chi^{(2)}_{\mathrm{abb}} = \chi^{(2)}_{\mathrm{acc}} = \chi^{(2)}_{\mathrm{bab}} = \chi^{(2)}_{\mathrm{bba}} = 1.2\ \mathrm{pm{\cdot}V^{-1}}$ (usually neglected) at 1064 nm, where a- and b-(c-) axes are parallel and perpendicular to the polar direction, respectively. Since a-axis is always parallel to the director of the local FNLC molecules, the local second-order nonlinear tensor elements can be calculated by transformation[2,3]:

$$\chi^{(2)}_{ijk}(z_0) = \sum_{ijk} \Omega(z_0)_{il}\,\chi^{(2)}_{lmn}\left[\Omega^{-1}(z_0)\right]_{mj}\left[\Omega^{-1}(z_0)\right]_{nk}, \tag{11}$$

where $i, j, k = \{x', y', z'\}$ is the local coordinate system, and the rotation matrices are given by

$$\mathbf{\Omega}(z_0) = \begin{pmatrix} \cos\theta(z_0) & \sin\theta(z_0) & 0 \\ -\sin\theta(z_0) & \cos\theta(z_0) & 0 \\ 0 & 0 & 1 \end{pmatrix}, \quad \mathbf{\Omega}(z_0)^{-1} = \begin{pmatrix} \cos\theta(z_0) & -\sin\theta(z_0) & 0 \\ \sin\theta(z_0) & \cos\theta(z_0) & 0 \\ 0 & 0 & 1 \end{pmatrix}, \tag{12}$$

The generation rate of photon pairs can be obtained by integrating:

$$R_{\mathrm{SPDC}} = \left[\int_0^L \sum_{lmn} \zeta_{lmn}(z)e^{i\Delta k z}dz\right]^2 \propto \left[\int_0^L \sum_{lmn} \chi^{(2)}_{lmn}(z)J_{p,lm}(z)E_{p,m}(z)e^{i\Delta k z}dz\right]^2, \tag{13}$$

where the Jones matrix $\boldsymbol{J}_p(z) = e^{-ik_p z}\boldsymbol{R}(z)\boldsymbol{M}_p(z)$ is consistent with Eq. (4).

Next, we consider the polarization evolution of the pump light $\left(A_{p,x}(0), A_{p,y}(0)\right)^T = a_p\left(\cos\theta_{\mathrm{pol}}, \sin\theta_{\mathrm{pol}}\right)^T$ with polarization angle θ_{pol} and amplitude a_p. The pump light can be transformed to the local coordinate system of the head director orientation at the entry surface as

$$\begin{pmatrix} A_{p,x'}(0) \\ A_{p,y'}(0) \end{pmatrix} = a_p \begin{pmatrix} \cos(\theta_{\mathrm{pol}} - \theta_{\mathrm{head}}) \\ \sin(\theta_{\mathrm{pol}} - \theta_{\mathrm{head}}) \end{pmatrix}. \tag{14}$$

Recalling the optical rotation effect in Section 1, the $x'(y')$ component of incident light is parallel (perpendicular) to the incident director, and the polarization remains parallel (perpendicular) to the director as the light propagates through the LC,

$$\begin{pmatrix} A_{p,x'}(z_0) \\ A_{p,y'}(z_0) \end{pmatrix} = e^{-ik_p z_0}\left[e^{-i\Gamma_p(z_0)/2}A_{p,x'}(0)\begin{pmatrix} \cos\Phi(z_0) \\ \sin\Phi(z_0) \end{pmatrix} + e^{i\Gamma_p(z_0)/2}A_{p,y'}(0)\begin{pmatrix} -\sin\Phi(z_0) \\ \cos\Phi(z_0) \end{pmatrix}\right]. \tag{15}$$

Note that the nonlinear coefficient $\chi^{(2)}_{\mathrm{aaa}}$ is only considered, and *a*-axis is always parallel to the director of the local FNLC molecules ($a//x'$). Therefore, in the SPDC process, we only consider the interaction between the *x*' component of the pump light and $\chi^{(2)}_{\mathrm{aaa}}$:

$$\begin{aligned}\chi^{(2)}_{aaa}\boldsymbol{e}_{aaa}(z_0)\bullet\begin{pmatrix}A_{p,x'}(z_0)\\A_{p,y'}(z_0)\end{pmatrix}&=\chi^{(2)}_{aaa}\begin{pmatrix}\cos\Phi(z_0)\\\sin\Phi(z_0)\end{pmatrix}\bullet\begin{pmatrix}A_{p,x'}(z_0)\\A_{p,y'}(z_0)\end{pmatrix}\\&=a_p\chi^{(2)}_{aaa}e^{-ik_pz_0}e^{-i\Gamma_p(z_0)/2}\cos(\theta_{\mathrm{head}}-\theta_{\mathrm{pol}})\end{aligned}, \tag{16}$$

where $\boldsymbol{e}_{aaa}(z_0)$ is the unit vector at $z = z_0$, and $\bullet$ represents the dot product. The generation rate of photon pairs can be obtained by integrating:

$$R_{\mathrm{SPDC}}=\left[\int_0^L a_p e^{-ik_pz}e^{-i\Gamma_p(z)/2}e^{i\Delta kz}\chi^{(2)}_{aaa}\cos(\theta_{\mathrm{head}}-\theta_{\mathrm{pol}})dz\right]^2. \tag{17}$$

Then, under the assumption of degenerate conditions for the down converted photons and the slowly varying amplitude approximation, the coincidence rate of the helical quasi-phase-matching is derived:

$$R_{\mathrm{SPDC}}\propto P_{\mathrm{pump}}d_{33}^2\cos^2(\theta_{\mathrm{head}}-\theta_{\mathrm{pol}})\cdot L^2\mathrm{sinc}^2\left(\frac{\Delta k_{\mathrm{HPM}}L}{2}\right). \tag{18}$$

where $d_{33}=\frac{1}{2}\chi^{(2)}_{aaa}$ is the dominant second-order nonlinear susceptibility of LC, $P_{\mathrm{pump}}\propto a_p^2$ is the pump power.

Next, we consider the polarization evolution of the photon pairs quantum state. The generated down-converted photon pairs of each thin layer undergo the optical rotation process from $z = z_0$ to $z = L$, we can obtain the quantum state of the exit surface through a treatment similar to that of the pump light,

$$\left|\psi(L-z_0)\right\rangle=\left[\boldsymbol{J}(L-z_0)\otimes\boldsymbol{J}(L-z_0)\right]\left|\psi'(z_0)\right\rangle. \tag{19}$$

where the Jones matrix $\boldsymbol{J}_j(L-z_0)=e^{-ik_j(L-z_0)}\boldsymbol{R}(L-z_0)\boldsymbol{M}_j(L-z_0)$ is consistent with Eq. (4), $\otimes$ represents the tensor product. Then, the overall quantum state of photon pairs generated by multilayer helical FNLC should be derived by integrating Eq. (9) within the thin-films region:

$$\left|\psi(d_1,d_2,\cdots,d_N)\right\rangle=\int_0^L\frac{d\left|\psi(z)\right\rangle}{dz}dz. \tag{20}$$

The generated states in Eq. (20) can be written in four orthogonal polarization bases:

$$\left|\psi\right\rangle=C\left[a_1e^{i\phi_1}\left|\mathrm{HH}\right\rangle+a_2e^{i\phi_2}\left|\mathrm{HV}\right\rangle+a_3e^{i\phi_3}\left|\mathrm{VH}\right\rangle+a_4e^{i\phi_4}\left|\mathrm{VV}\right\rangle\right], \tag{21}$$

where $C=\left(\left|a_1\right|^2+\left|a_2\right|^2+\left|a_3\right|^2+\left|a_4\right|^2\right)^{-\frac{1}{2}}$. The density matrix of the state is $\boldsymbol{\rho}=\left|\psi\right\rangle\left\langle\psi\right|$.

Section 3: Helical QPM vs. periodically poled QPM

Typically, the periodically poled nonlinear crystals have a fixed period and binary poled direction, corresponding to the desired phase matching process. However, domain walls may be non-planar and other defects may occur within the domains, depending on the poling technique[4]. These effects cause losses and decrease nonlinear efficiency. The helical structure of FNLC has a periodic structure and can similarly provide a reciprocity vector for the nonlinear phase matching process. In contrast to periodically poled crystal, helical FNLC does not generate defect lines and non-planar domain wall along the propagation direction due to the continuous periodic structure and self-assembly characteristics.

Another important aspect is the difference in Fourier purity between helical quasi-phase matching (QPM) and periodically poled QPM. The QPM Fresnel series is described as follows. Spatial dependence of the nonlinear coefficient $d(z)$ of periodically poled QPM can be considered as a square wave function and can be expressed in terms of a Fourier series as[5]

$$d(z) = d_{eff} \sum_{m=-\infty}^{\infty} b_m e^{iG_m z}, \tag{22}$$

where the Fourier coefficients are given by $b_m = 2/m\pi$, $G_m = 2\pi m/\Lambda$ is the reciprocity vector of the odd m-th Fourier component. It can be found that the Fourier series has non-negligible high-order components, most of the components provide a reciprocity vector which is not helpful for phase matching.

In the case of helical QPM, $d(z)$ can be considered as a cosine wave function and the Fourier coefficients are

$$b_m = \tfrac{1}{2}\left(\delta_{m,1} + \delta_{m,-1}\right), \tag{23}$$

where δ is the Kroneker delta function, and there are non-zero coefficients only when $m = \pm 1$. This sinusoidal modulation produces only first-order Fourier components without higher-order harmonics. Thus, the helical polarization in the phase matched FNLC has high Fourier purity, which helps to avoid the efficiency loss and the noise photons caused by the other nonlinear process corresponding to the high-order Fresnel coefficients.

Section 4: Nonreciprocal quantum SPDC in orthogonally aligned FNLC

We can see from the Eq. (18) that the SPDC emission efficiency is governed by the relationship between linear polarization angle θ_{pol} and orientation angle of head LC θ_{head}. The polarization angle dependence is shown in **Fig. S2**. For the single-side linear incidence, the maximum generation rate occurs at $\theta_{pol} // \theta_{head}$ and a minimum rate at $\theta_{pol} \perp \theta_{head}$, whereas an orthogonal director orientation yields minimal generation. When the incident direction is reversed, the coincidence rate depends on the relationship between linear polarization angle θ_{pol} and orientation angle of tail LC θ_{tail}. Then, for the same incident parameters, the coincidence rate of the forward and backward incidence can be derived as:

$$R_{\mathrm{Foward}} \propto P_{\mathrm{pump}} d_{33}^2 \cos^2(\theta_{\mathrm{head}} - \theta_{\mathrm{pol}}) L^2 \mathrm{sinc}^2\left(\frac{\Delta kL}{2}\right), \tag{24a}$$

$$R_{\mathrm{Backward}} \propto P_{\mathrm{pump}} d_{33}^2 \cos^2(\theta_{\mathrm{tail}} - \theta_{\mathrm{pol}}) L^2 \mathrm{sinc}^2\left(\frac{\Delta kL}{2}\right). \tag{24b}$$

Under the phase matching condition $\Delta k \approx 0$, the nonreciprocal isolation ratio is

$$\begin{aligned} \mathrm{Isotation}\,(\mathrm{dB}) &= 10\log_{10}\left(R_{\mathrm{Forward}} / R_{\mathrm{Backward}}\right) \\ &= 10\log_{10}\left(\cos^2(\theta_{\mathrm{head}} - \theta_{\mathrm{pol}}) / \cos^2(\theta_{\mathrm{tail}} - \theta_{\mathrm{pol}})\right) \end{aligned}. \tag{25}$$

For an orthogonal alignment boundary conditions (H- and V-oriented anchoring at head and tail, respectively), the nonreciprocal isolation ratio is simplified to

$$10\log_{10}\left(\tan^2\theta_{\mathrm{pol}}\right). \tag{26}$$

Therefore, when the incident light polarization angle is π/2 (V polarization), the nonreciprocal isolation can reach the maximum value of infinite, and the minimum value of negative infinity can be obtained by H polarization incidence. It is worth noting that both the infinity and negative infinity values indicate extremely high nonreciprocity, because the isolation of the reciprocity is equal to 1, which can be obtained by diagonal linear polarization incidence.

For circularly polarized pumping, whether it is forward or backward incident, the polarization state that changes with propagation always maintains a significant component when projected to the direction of the effective nonlinear coefficient. Therefore, SPDC entangled photon pairs can always be effectively generated, and the isolation is reduced.

Section 5: Polarization state of quantum photon-pair.

The complete information of the polarization states can be described through the density matrix, which is reconstructed experimentally by the standard quantum tomography technology. For a two-photon polarization state, there are 16 independent variables considering the positive semidefinite Hermitian matrix, corresponding to the measurements with 16 self-contained orthogonal basis[6]. And the maximum likelihood estimation is used in the calculations to resist from the measurement noise[7].

Therefore, for a same HPM LC sample with orthogonal orientations of head and tail LC directors, the reconstructed density matrix for pump light with horizontal linear and diagonal linear are similar, as shown in **Fig. S7**. These results agree well with the theoretical ones, which demonstrate that the quantum polarization states under different polarized pump are basically parallel to the orientational angle of the exit surface, superposed by mostly |VV⟩ photon state and a small fraction of |HV⟩ state. This pump polarization-independent twin photon polarization state can be understood from the discussion in Section 2.

For an HPM FNLC with a fixed director at incidence surface and a varying director at exit surface, we further calculated the corresponding quantum polarization states of the SPDC photon pairs as shown in **Fig. S8**. It can be observed that the generated two-photon polarization states are mostly parallel to the tail director at the exit surface, which consists with the aforementioned analysis since the generated SPDC photons also rotate with the helix structure of FNLC till the end. Therefore, we can summary that the brightness of the photon pairs only dependent on the pitch, the length and the relationship between θ_{head} and θ_{pol}, while the polarization state of the photon pairs only dependent on the orientation of the FNLC at the exit surface. The polarization states of the generated SPDC photons are noticed to be usually not perfect pure states or maximum polarization entangled states for the HPM FNLC, and an HPM FNLC-based efficient maximum polarization entangled photon source might be achieved by post-selection with the Sagnac ring setup.

Section 6: Dynamically tunable SPDC

In this section, we show the thermally and electrically modulations of brightness of entangled photon pairs. The thermal phase sequence of the FNLC includes the isotropic phase, nematic phase, and ferroelectric nematic phase, and the three phases correspond to the temperatures from high to low. The FNLC material crystalizes around 40 °C, a temperature that can vary depending on the cooling rate[3]. For a linear polarized pumping light, the coincidence rate as a function of temperature is shown in **Fig. S9a**. When the LC device is in the isotropic and nematic phase, no signal is obtained due to the disappearance of the ferroelectricity and the zero second-order magnetic susceptibility After entering the ferroelectric nematic phase (temperature decreases below 128 °C), the coincidence rate of the photon pairs increases rapidly at the beginning, then shows a slow growth, and ultimately reaches a saturation of about 10^4 pairs/s.

In addition, we demonstrate the electrically modulation of SPDC. In the experiment, a sinusoidal wave AC electric field is vertically applied to the LC device. When external low-frequency electric field is vertically applied, the spontaneous polarization of FNLC undergoes electrical realignment[3], leading to the change of reciprocal vector *G* provided by the helical structure. **Figure S9b** demonstrates the periodic switching of the coincidence rate, with the modulation frequency of 20 Hz and the electric field amplitude of 0-20 mV/μm. Furthermore, a method of changing the periodic frequency of SPDC by varying the applied electric field signal, is achieved by dynamically changing the modulation frequency from 0.5 Hz to 1 Hz with the electric field amplitude of 0-80 mV/μm, as shown in **Fig. S9c**.

Supplementary Figures:

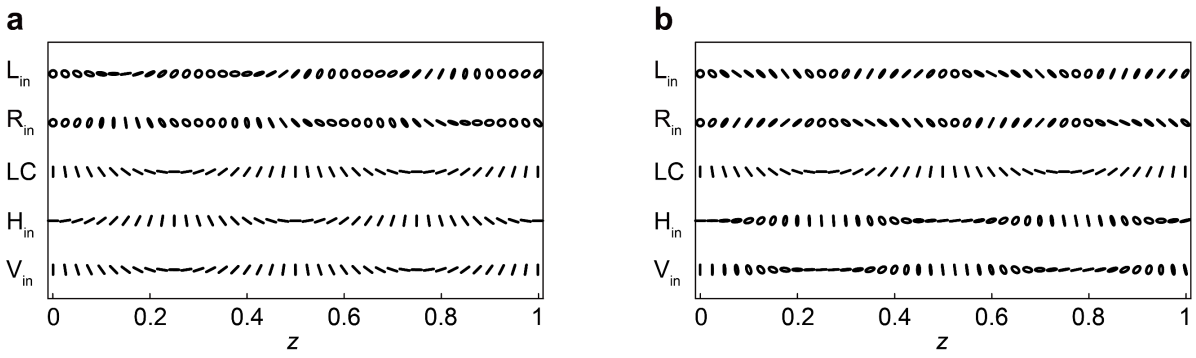

Fig. S1 | Optical rotatory effect of the helical FNLC. The evolution of the polarization with vertical (V), horizontal (H), left-handed circular (L), and right-handed circular (R) polarized incident polarization conditions for ideal situation (**a**) and experimental situation (**b**).

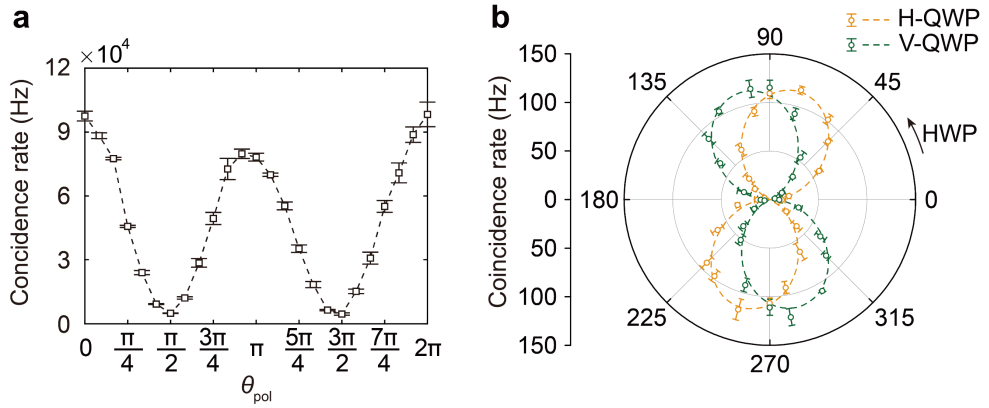

Fig. S2 | Polarization-dependent photon-pair coincidence rate. Coincidence rate as a function of linear polarization angle (**a**) and elliptical polarization (**b**). A polarization control system comprising a linear polarizer (LP) and a quarter-wave plate (QWP) enables continuous tuning of the incident polarization state, spanning linear, circular, orthogonal linear, and opposite circular polarizations.

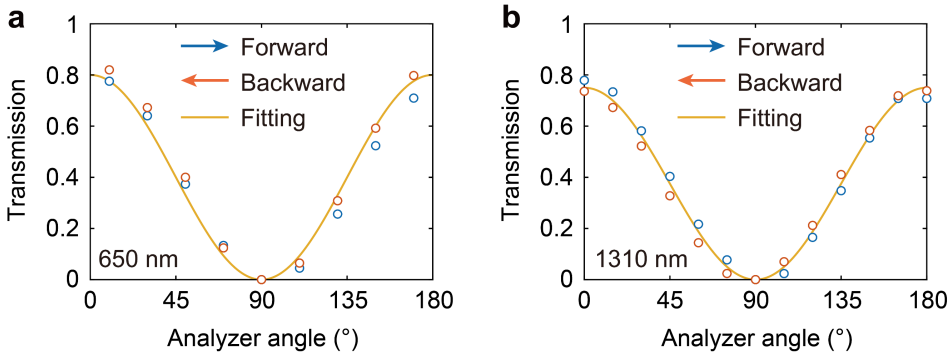

228

229 **Fig. S3 | Reciprocal transmittance for classical linear case.** The transmittance of 650 nm (**a**) and 1310 nm
230 (**b**) versus the analyzer angle for different input directions. The incident polarization is along to V direction.

231

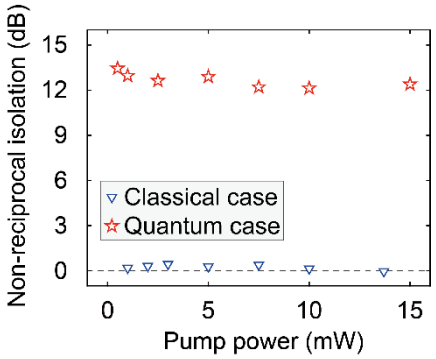

Fig. S4 | Isolation contrast between classical and quantum cases. Classical case exhibits ~0 dB isolation with transmission. Nonreciprocal quantum case achieves a high isolation ~13 dB.

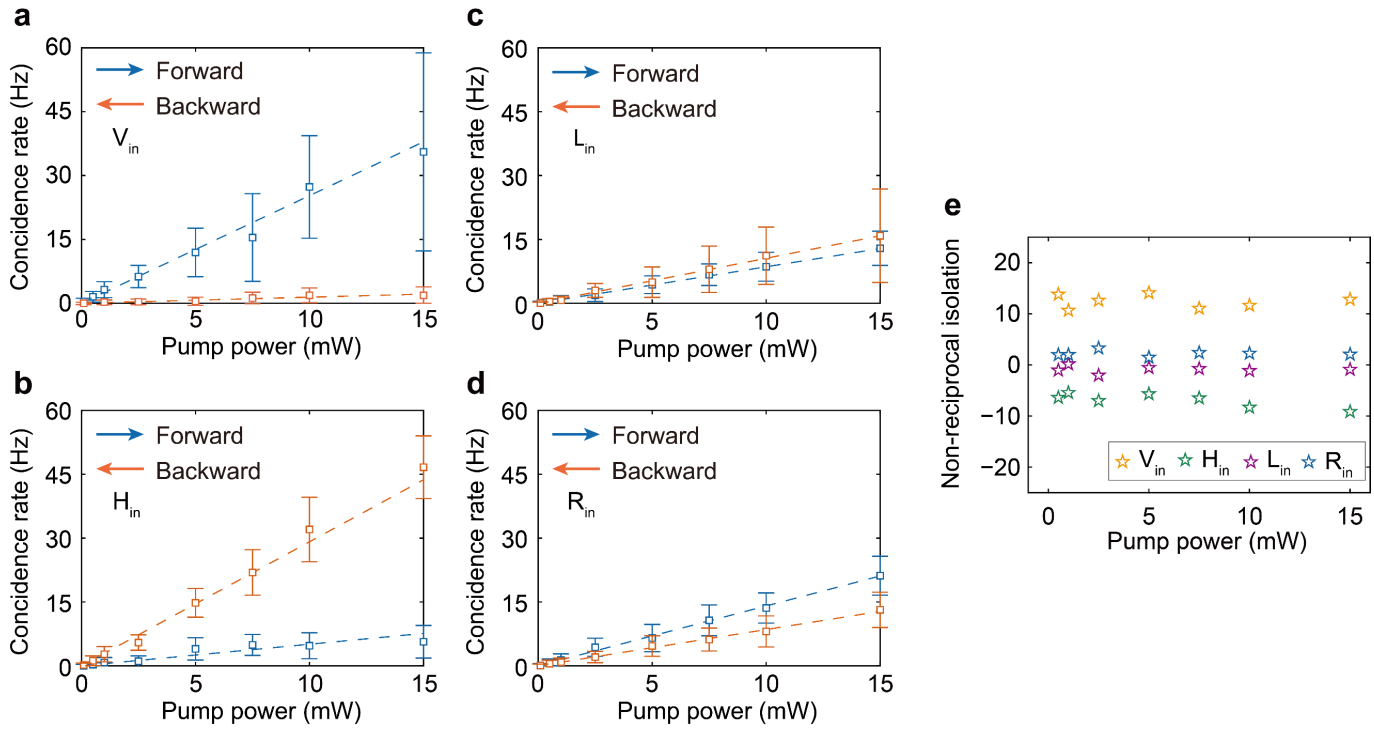

236

237 **Fig. S5 | Nonreciprocal quantum SPDC in non-phase matched FNLC. a-d**, Forward and backward SPDC
238 coincidence rates versus pump power for non-reciprocal SPDC under vertical (V), horizontal (H), left-handed
239 circular (L), and right-handed circular (R) polarized pumping. **e**, Isolation contrast for non-reciprocal SPDC
240 under V, H, L, and R polarized pumping. Here, the boundary condition of the FNLC is orthogonally aligned.

241

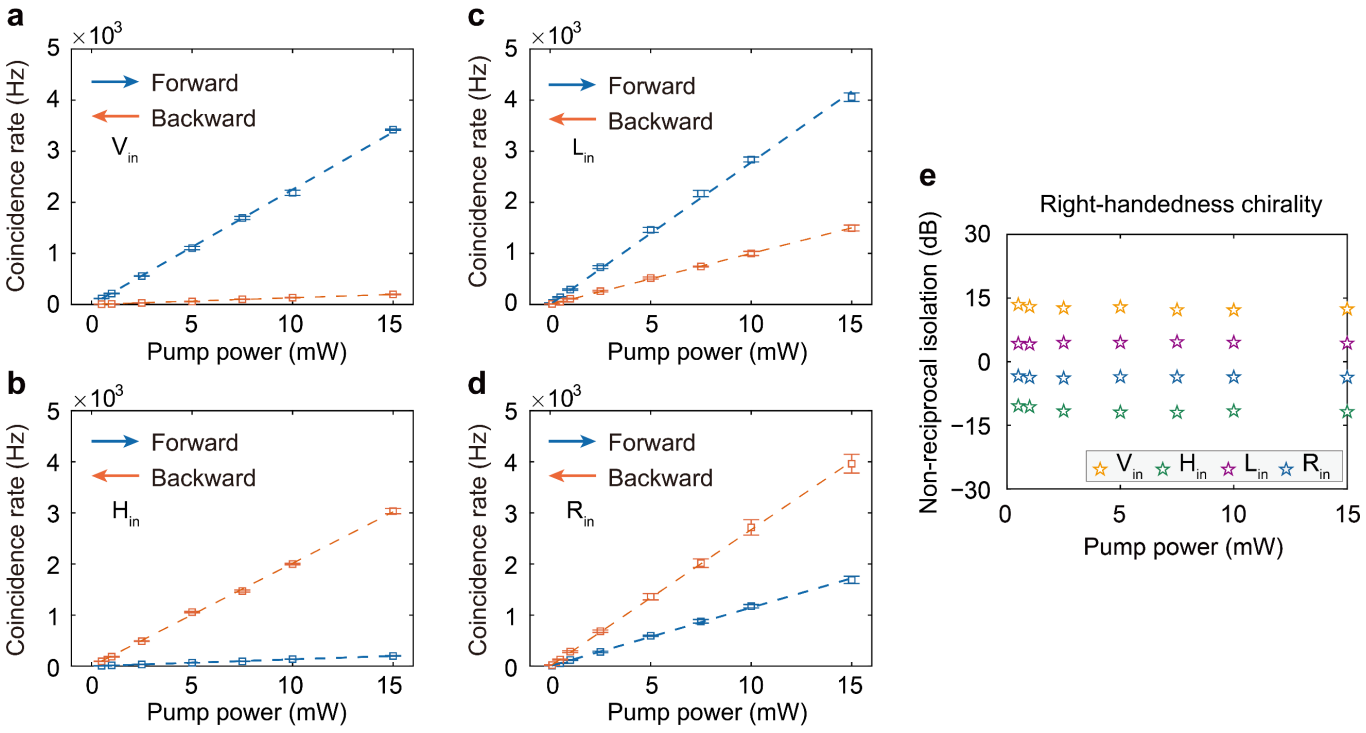

Fig. S6 | Nonreciprocal quantum SPDC in right-handed phase matched FNLC. a-d, Forward and backward SPDC coincidence rates versus pump power for non-reciprocal SPDC under V, H, L, and R polarized pumping. **e**, Isolation contrast for non-reciprocal SPDC under V, H, L, and R polarized pumping. Here, the boundary condition of the FNLC is orthogonally aligned.

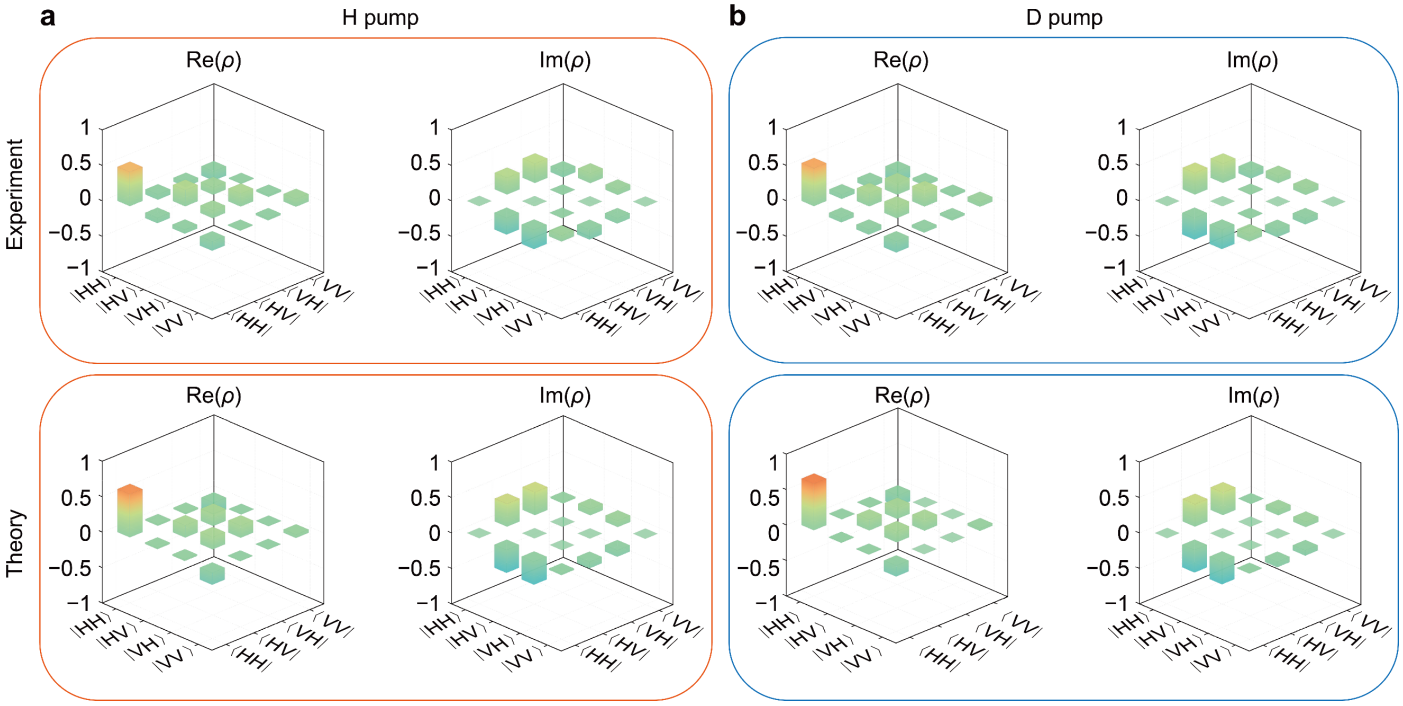

Fig. S7 | Biphoton polarization states under different pumping polarization. Experimental and theoretical polarization density matrices under H-polarized (**a**) and D-polarized ($\theta_{pol} = \pi/4$) (**b**) pumping.

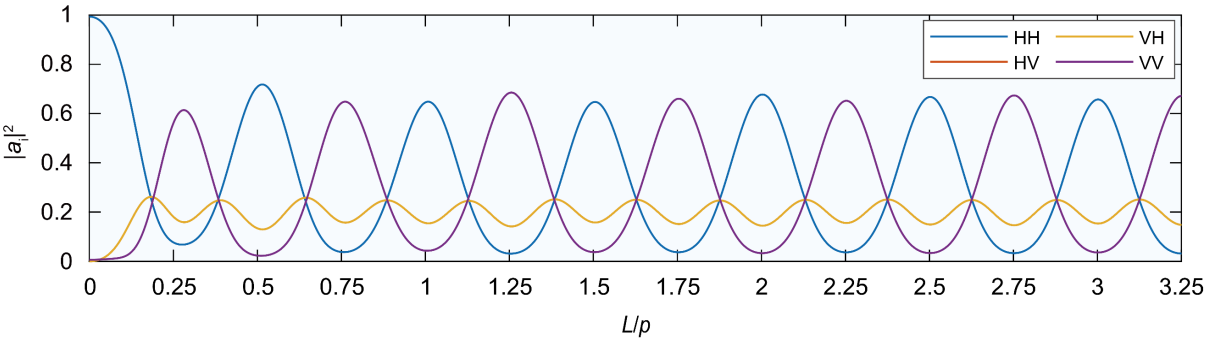

Fig. S8 | Calculated quantum polarization states of the SPDC photon pairs. Polarization states of the generated photon pairs as a function of thickness-to-pitch ratio, showing the generated two-photon polarization states are mostly paralleled to the tail director at the exit surface.

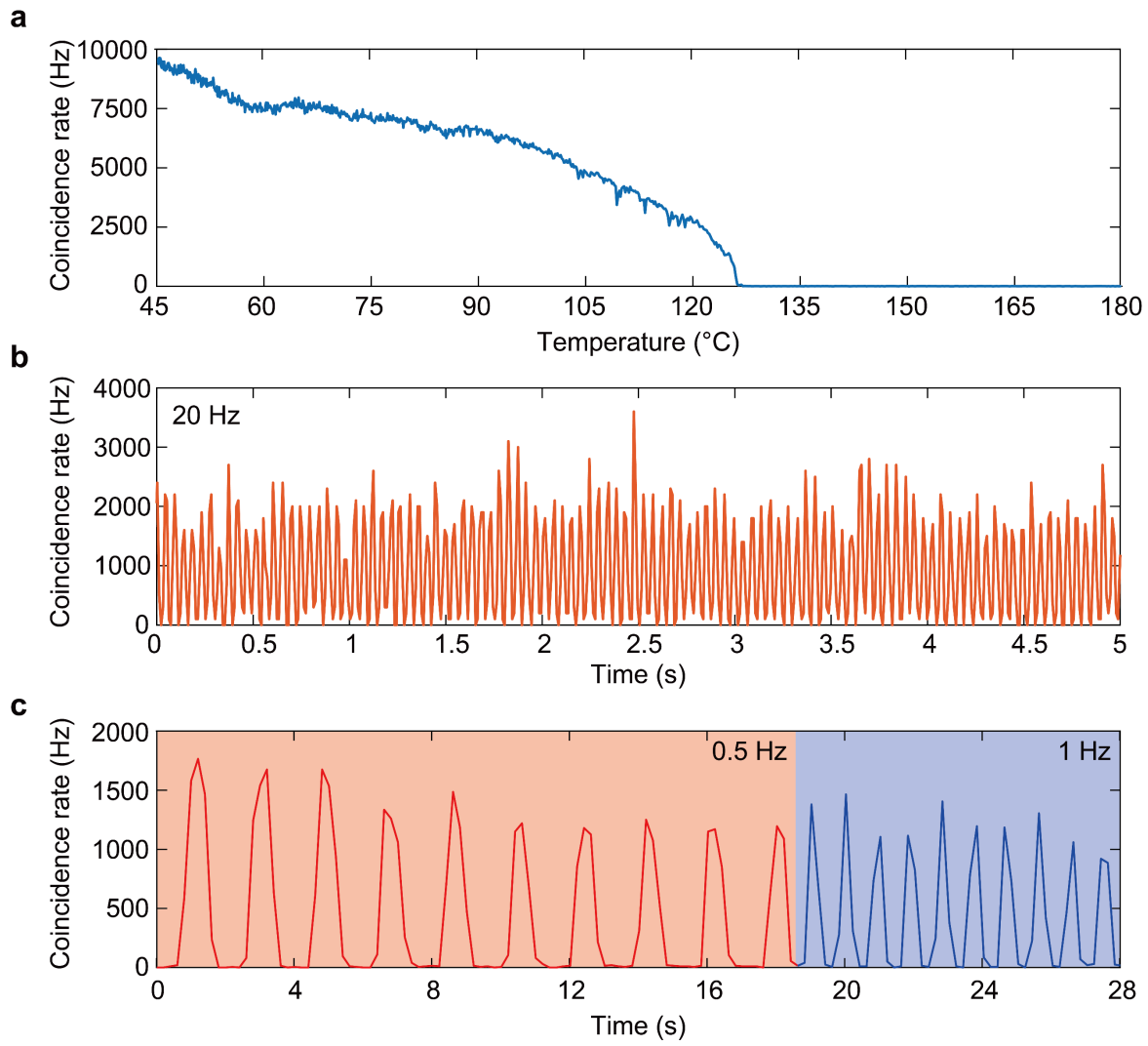

Fig. S9 | Dynamically tunable photon pairs of the helical FNLC. a, Thermally tunable coincidence rate. **b**,**c**, Periodic switching of the coincidence rate by electrically tuning the spontaneous polarization of the helical phase matched FNLC, leading to the change of reciprocal vector *G* provided by the helical structure.

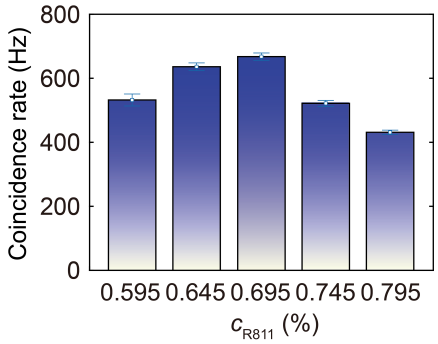

Fig. S10 | The coincidence rates as a function of the concentration of R811. The optimized concentration of the chiral agent used in the main text for HPM was 0.695 wt%.

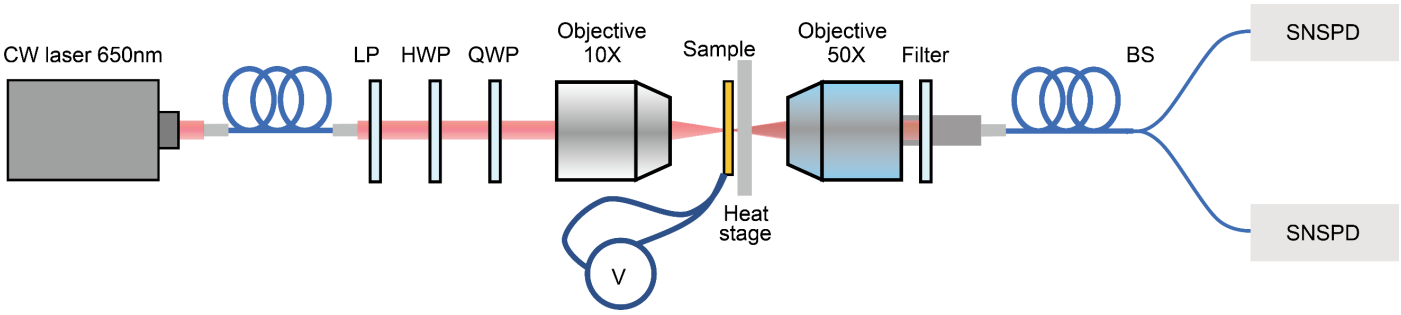

Fig. S11 | Optical setup for the photon-pair generation and correlation measurements. Generated photon pairs generated by 650 nm pumping were detected via coincidence SNSPD measurements. HWP, half-wave plate; QWP, quarter-wave plate; LP, linear polarizer; BS, fiber beam-splitter; SNSPD, superconducting nanowire single-photon detector.

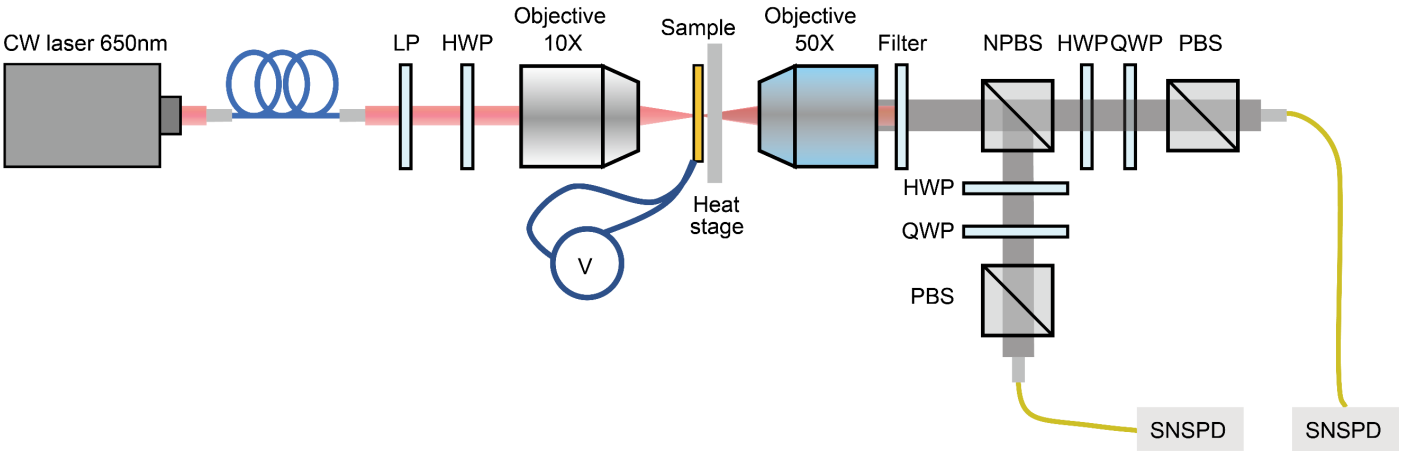

272

273 **Fig. S12 | Optical setup for quantum tomography.** LP, linear polarizer; HWP, half-wave plate; QWP,
274 quarter-wave plate; NPBS, non-polarizing beam-splitter; PBS, polarizing beam-splitter; BS, fiber beam-
275 splitter; SNSPD, superconducting nanowire single-photon detector.

276

Supplementary References

1. Yang, D.-K. & Wu, S.-T. *Fundamentals of liquid crystal devices*. (John Wiley & Sons, 2014).
2. Guo, Q. *et al.* Polarization entanglement enabled by orthogonally stacked van der Waals $NbOCl_2$ crystals. *Nat. Commun.* **15**, 10461 (2024).
3. Pan, J.-T. *et al.* Nonlinear geometric phase coded ferroelectric nematic fluids for nonlinear soft-matter photonics. *Nat. Commun.* **15**, 8732 (2024).
4. Kitaeva, G. K. *et al.* Mapping of periodically poled crystals via spontaneous parametric down-conversion. *Appl. Phys. B* **81**, 645–650 (2005).
5. Boyd, R. W. *Nonlinear optics*, 3rd edn. (Academic Press, 2008).
6. James, D. F. V., Kwiat, P. G., Munro, W. J. & White, A. G. Measurement of qubits. *Phys. Rev. A* **64**, 052312 (2001).
7. Banaszek, K., D'Ariano, G. M., Paris, M. G. A. & Sacchi, M. F. Maximum-likelihood estimation of the density matrix. *Phys. Rev. A* **61**, 010304 (1999).